MOL #51706

**STI571-Induced Cell Edge Translocation of Kinase-Active and Kinase-Defective Abl: Requirements of Myristoylation and SH3 Domain**

Akiko Fujita, Tomoyuki Shishido, Yunfeng Yuan, Eiji Inamoto, Shuh Narumiya and Naoki Watanabe

A.F., Y.Y., E.I., S.N., N.W.

Department of Pharmacology, Kyoto University Faculty of Medicine

Yoshida Konoe-cho, Sakyo-ku, Kyoto 606-8501, Japan

T.S.

Laboratory of Molecular Oncology, Nara Institute of Science and Technology,

8916-5 Takayama, Ikoma, Nara 630-0192, Japan

**Running Title: STI571-Induced Cell Edge Translocation of Abl**

Corresponding author: Naoki Watanabe

Department of Pharmacology, Kyoto University Faculty of Medicine

Yoshida Konoe-cho, Sakyo-ku, Kyoto, Japan 606-8501

Tel: +81-75-753-4396, Fax: +81-75-753-4693

E-mail: naoki-w@mfour.med.kyoto-u.ac.jp

The number of text pages: 37 pages

0 tables

6 figures

45 references

248 words in Abstract

653 words in Introduction

1088 words in Discussion

**Abbreviations:** STI571 (imatinib mesylate, Gleevec or Glivec), 4-[(4-Methyl-1-piperazinyl)methyl]-N-[4-methyl-3-[[4-(3-pyridinyl)-2-pyrimidinyl]amino]-phenyl]benzamide methanesulfonate; Abl, Abelson kinase; Bcr, break-point cluster region; EGFP, enhanced green fluorescent protein; EGFR, epidermal growth factor receptor; CML, chronic myelogenous leukemia; SH3, src homology 3; Mena, mammalian Enabled; 3BP1, SH3-domain binding protein 1; abi-1, abl-interactor 1; pag, proliferation-assoicated gene; MSP23, macrophage 23-kD stress protein; FRET, fluorescence resonance energy transfer; BRET, bioluminescence resonance energy transfer; Crk, v-crk sarcoma virus CT10 oncogene homolog; PKA, cyclic AMP-dependent kinase; Sra, specifically Rac-associated protein, Nap1, Nck-associated protein 1; Rb, retinoblastoma protein.

## ABSTRACT

STI571 is the first successful target-based drug with excellent potency against chronic myelogenous leukemia. Studies on this compound have illuminated potentials and problems of kinase inhibitors in the treatment of cancer. As found in crystal structures, STI571-bound abl is believed to form closed conformation with N-terminal regulatory domains. Here we present evidence of distinct STI571-induced modulation of abl functions using high-resolution live-cell imaging approaches. Within lamellipodia of fibroblast cells, STI571 was found to induce rapid translocation of abl to the lamellipodium tip. Quantitative analysis yielded 0.81 μM and 1.8 μM for $EC_{50}$ of STI571-induced cell edge translocation of abl-KD-GFP and wild-type abl-GFP, respectively. It also revealed adverse response of drug-resistant abl-T334I to STI571, suggesting that drug binding to abl-GFP triggers translocation. N-myristoylation and the SH3 domain were required for this translocation whereas disruption of intramolecular interactions of these motifs enhanced cell edge association of abl. An intact C-terminal last exon region in abl, but not its F-actin binding, was required for efficient cell edge translocation. Moreover, single-molecule observation revealed an STI571-induced rapid increase in slow diffusive species of abl in both the tip and the body region of lamellipodia. These results suggest that while activated abl translocates to the cell edge at its open state, STI571 can also bind and lock abl in the open and membrane-tethered conformation as long as the SH3 domain and the C-terminal region are intact. High resolution imaging can be a powerful tool for elucidating inhibitor modulation of abl functions under intracellular environment.

## Introduction

Abl is a non-receptor tyrosine kinase which is implicated in cellular processes such as cell-substrate adhesion, apoptosis, cell cycle regulation and stress response (Pendergast, 2002; Suzuki and Shishido, 2007). Expression of a chimeric Bcr-abl protein, which arises from a reciprocal translocation between chromosomes 9 and 22, causes chronic myelogenous leukemia (CML) (de Klein et al., 1982). STI571, also called imatinib or Gleevec, induces hematologic remissions in 90% of patients in chronic phase of CML (Kantarjian et al., 2002). However, patients receiving this drug may develop drug resistance associated with kinase domain mutations. This led to development of novel abl kinase inhibitors with a higher potency and broader inhibition spectrums against mutated kinases (Quintas-Cardama et al., 2007). However, several mutations remain resistant to new inhibitors.

In abl, NCAP, SH3 and SH2 domains precede the kinase domain (Woodring et al., 2003). In abl Ib, a major splice variant of c-abl in human (type IV in mouse), the NCAP region is myristoylated. This myristoylated N-terminal peptide binds the kinase C-lobe (Hantschel et al., 2003; Nagar et al., 2003), conferring autoinhibited conformation of abl. The SH3 domain also plays an important role, forming a bridge with the linker between SH2 and kinase domains in auto-inhibited abl (Barila and Superti-Furga, 1998). The SH3 domain also interacts with several ligands such as Abi-2, 3BP-1 and Pag/MSP23 (Cicchetti et al., 1995; Dai and Pendergast, 1995; Wen and Van Etten, 1997). An *in vitro* random mutagenesis analysis of Bcr-abl has identified mutations that give rise to STI571 resistance not only in the kinase domain but also in these N-terminal regulatory domains (Azam et al., 2003). Notably, several residues conferring STI571 resistance in Bcr-abl are identical to the residues that convert c-abl to an oncogene (Barila and

Superti-Furga, 1998; Brasher and Van Etten, 2000; Van Etten et al., 1995), suggesting a common mechanism for drug susceptibility between Bcr-abl and c-abl. Such regulatory domain mutations appear to destabilize the autoinhibited conformation (Azam et al., 2003). In crystals (Nagar et al., 2006; Nagar et al., 2003; Schindler et al., 2000), N-terminal regulatory domains in the STI571-bound abl form a closed autoinhibited conformation. It is therefore widely accepted that STI571 stabilizes the closed conformation of the N-terminal half of abl.

With regard to the C-terminus downstream of the kinase domain, its F-actin binding downregulates the kinase activity (Hantschel et al., 2005; Woodring et al., 2001). Through proline-rich motifs between the kinase and the C-terminal F-actin binding domains, abl interacts with abi-1 and abi-2 (Dai and Pendergast, 1995; Shi et al., 1995) which bridge the association with its substrate, Mena (Tani et al., 2003). Although the structure of full-length abl has not been solved and the precise relationship between the kinase and the F-actin binding domains remains to be elucidated, the association of abl with F-actin and its regulatory proteins may have close relationship with regulation of its kinase activity.

Cell imaging-based assays involving $Ca^{++}$ indicators, chemiluminescence, FRET/BRET and phosphorylation-specific antibodies can be useful tools for drug development and drug target evaluation. They enable rapid assay preparation by eliminating steps of protein purification and biochemical reconstitution. They may include all required components in assay systems. However, it is often problematic to distinguish whether drugs exert the effect directly or secondarily through distinct targets. For example, Crk-II based FRET probes change the emission profile upon phosphorylation by either abl or EGFR (Kurokawa et al., 2001; Ting et al., 2001). Here

we report a more versatile method to monitor drug modulation of abl functions that is direct observation of molecular behaviour of GFP-tagged abl using high resolution fluorescence microscopy. We show that STI571 induces rapid translocation of abl to the tip of lamellipodia in fibroblast cells. We have developed several quantitative analysis methods including single-molecule observation (Miyoshi et al., 2006; Watanabe and Mitchison, 2002). Our domain analysis within the abl structure reveals STI571-induced rapid cell edge translocation of abl possibly through promoting complex formation with putative cellular partner(s).

MOL #51706

**Materials and Methods**

**Plasmids and reagents.**

pcDNA3-abl and pcDNA3-ablKD encoding cDNA of murine type IV c-abl and its kinase defective K290M mutant, abl-KD, were provided by David Baltimore. mRFP1 (Campbell et al., 2002) and mCherry cDNAs (Shaner et al., 2004) are gifts from Roger Y. Tsien. For preparation of wild-type and deletion mutants of abl, appropriate fragments of abl cDNA were amplified by PCR and introduced into pEGFP vectors (Clontech Laboratories, Mountain View, CA). Point mutations were introduced using Quick Change site-directed mutagenesis kit (Stratagene, La Jolla, CA). For mRFP1 fusion constructs, the coding region of EGFP was replaced by mRFP1 cDNA. The expression vector for mCherry-actin was generated by substituting mCherry cDNA for the coding sequence of EGFP in delCMV-EGFP-actin (Watanabe and Mitchison, 2002). The abl inhibitor, STI571, was supplied by Novartis Pharma (Basel, Switzerland).

**Live cell imaging and fluorescence single-molecule observation.**

Live cell imaging and single-molecule observation were carried out as described (Miyoshi et al., 2006; Watanabe and Mitchison, 2002). Briefly, *Xenopus* XTC fibroblasts were transfected using SuperFect (Qiagen, Valencia, CA) and maintained after passage into fresh flasks. Before experiments, cells were trypsinized and allowed to spread on a poly-L-lysine (1 mg/ml)-coated glass coverslip attached to a handmade flow cell in 70% Leibovitz's L15 medium (Invitrogen, Carlsbad, CA) without serum for 30 min. The flow cell was placed on the stage of Olympus (Tokyo, Japan) BX52, BX51 or IX71 microscope equipped with a cooled CCD camera; RTE/CCD-1300-YHS (Roper Scientific), Cascade II:512 (Roper Scientific, Princeton, NJ) or UIC-QE (Molecular

7

Device, Sunnyvale, CA). Fluorescence images were acquired at 21-23 °C using the Metamorph software (Molecular Device) and Olympus objectives, PlanApo 100× (NA 1.40) or UApo 150×O TIRFM (NA 1.45) up to 120 min after cells were seeded. For fluorescence single-molecule speckle microscopy, illumination was restricted to the cell peripheral areas. Single-molecule counting was carried out manually.

**Immunofluorescence analysis**

XTC cells transfected with pcDNA3-abl, an expression construct encoding full-length murine type IV c-abl (Tani et al., 2003), were trypisinized and allowed to spread onto poly-L-lysine-coated glass coverslips for 45 min as described above. Cells were then incubated in the medium with or without 1 μM STI571 for 5 min, and fixed in Cytoskeleton buffer (10 mM MES, [pH 6.1], 90 mM KCl, 3 mM $MgCl_2$, 2 mM EGTA, 0.16 M sucrose) containing 3.7% paraformaldehyde for 20 min at room temperature. The samples were then permeabilized by 0.2% Triton X-100 in Tris buffered saline (10 mM Tris pH 7.5, 150 mM NaCl). A rabbit polyclonal anti-abl antibody (Cell Signaling Technology, Danvers, MA) was used at 1:100 dilution for the primary antibody. Alexa fluor 594 anti-rabbit antibody and Oregon Green 488 phalloidin (Invitrogen, Carlsbad, CA) were used to visualize the primary antibody and filamentous actin, respectively. Images were acquired using Olympus BX52 epifluorescence microscope and PlanApo 60× TIRFM (NA 1.45).

## Results

### STI571 induces cell edge translocation of abl-GFP probes.

We fused type IV mouse c-abl with fluorescent proteins (EGFP or mRFP1) at its C-terminus and expressed it in *Xenopus* XTC fibroblasts. These cells adhere tightly to poly-L-lysine-coated glass coverslips and form wide flat lamellipodia (Watanabe and Mitchison, 2002). Placing the cell periphery in a flat geometry enables precise microscopic observations of spatiotemporal regulation of cytoskeletal rearrangement and molecular behaviour (Miyoshi et al., 2006; Nakagawa et al., 2001; Watanabe and Mitchison, 2002). The merits of our model system also include the ease of cell culture under the microscope because cells grow at room temperature without supply of $CO_2$. We focused on the behavior of abl-EGFP at the cell periphery and found its association with the actin network throughout lamellipodia in XTC cells (Fig. 1A). In lamellipodia, the tip region was the most intensely labelled. These observations are consistent with the localization of endogenous abl (Jin and Wang, 2007; Woodring et al., 2002). When overexpressed, abl-EGFP induced the formation of finger-shaped actin-rich structures where abl-EGFP was associated. These abl-associated structures dynamically moved and often extended toward the cell periphery against the retrograde actin flow (supplementary Fig. 1 and Movie 1) which fluxes inward at ~1.5 μm/min (Watanabe and Mitchison, 2002). Previous studies have reported analogous effects of abl in the promotion of microspike formation (Woodring et al., 2002) and elongation of the actin comet tail induced by *Shigella flexneri* (Burton et al., 2005).

Previously, only the negligible effect of STI571 on the localization of abl has been reported (Hantschel et al., 2005). By observing abl-EGFP in wide flat lamellipodia, however, we noticed a rapid increase in abl-EGFP signals at the lamellipodium tip as

well as at dots in the lamellae region upon perfusion of STI571 (Fig. 1B, supplemental Movie 2). Simultaneously, a loss in abl-EGFP signals associated with the F-actin network was also observed. These observations suggest a decrease in the affinity between abl and F-actin as well as the increased affinity of abl to putative partner(s) at the lamellipodium tip induced by STI571.

We also verified that untagged full-length abl also translocated to the cell periphery in response to STI571 (Fig. 1C). These results exclude the possibility that the GFP-tag attached to the C-terminus of abl caused abnormal response to STI571 by alternating the open/closed conformational regulation of abl kinase.

Overexpression of abl-EGFP impaired spreading of XTC cells. STI571 relieved this inhibition and induced cell edge protrusion (Fig. 1B, lower panels). These observations are consistent with the impaired spreading of NIH3T3 cells by induced dimerization of abl-FKBP (Jin and Wang, 2007). The edge of non-transfected XTC cells protruded less markedly in response to STI571 (data not shown). These results suggested that overexpressed abl negatively regulates cell edge extension through excessive phosphorylation of its substrates. We therefore wondered whether STI571-induced translocation of abl occurred as a result of dephosphorylation of its substrates. To test this, we generated kinase-dead abl probes, abl-KD-EGFP and abl-KD-mRFP1, in which K290 was substituted to methionine. In contrast to wild-type, abl-KD-EGFP did not interfere with cell spreading. Only marginal lamellipodium extension was induced by STI571 treatment in cells expressing abl-KD constructs as in control cells, suggesting a low level of phosphorylation of abl substrates in abl-KD expressing cells (Tani et al., 2003). Upon perfusion of STI571, abl-KD rapidly translocated to the lamellipodium tip and cytoplasmic actin-rich foci to a similar degree as wild-type abl (Fig. 1D). Therefore,

dephosphorylation of abl substrates is unlikely to be the mechanism for its STI571-induced translocation.

We next verified that STI571-induced translocation is not caused by a change in F-actin morphology. Translocation of abl-KD occurred without substantial F-actin redistribution (Fig. 1E, supplemental Movie 3). We also confirmed that the accumulation of abl-KD-EGFP was not due to an increase in the thickness of the cell edge (Fig. 1F).

**Dose-response analysis of STI571-induced cell edge translocation of abl.**

Fig. 2A shows dose-response analysis of STI571-induced translocation of abl-KD. We measured the ratio of the EGFP fluorescence intensity between the edge and the body areas in lamellipodia (supplemental Movie 4, 5) by building a computer-aided quantification method. This method combines image manipulation and measurement commands in the MetaMorph software. This nonbiased analysis yielded 0.81 μM for $EC_{50}$ of STI571-induced translocation of abl-KD. This $EC_{50}$ is comparable to $IC_{50}$ of STI571 for the inhibition of abl in cell-based assays, 0.25-0.8 μM (Azam et al., 2003; Druker et al., 1996; Roumiantsev et al., 2002; Quintas-Cardama et al., 2007). We also carried out the same analysis on wild-type abl-EGFP (Fig. 2B). The $EC_{50}$ of STI571-induced cell edge translocation of wild-type abl was 1.8 μM, which is slightly higher than that of abl-KD. Especially at lower concentrations, 0.5-5 μM, STI571-induced cell edge translocation of wild-type abl was less marked than abl-KD. Phosphorylation at Y412 within the activation loop impairs STI571 binding to abl kinase with an increase in the $Ki$ value from 37 nM to 7 μM (Schindler et al., 2000). The importance of this phosphorylation has also been noted by the fact that mutation at P131

confers STI571-resistance in cells (Azam et al. 2003) although P131L mutation renders the kinase more sensitive rather than more resistant to STI-571 in its unphosphorylated state (Roumiantsev et al., 2002). We therefore speculated that autophosphorylation at Y412 (Brasher and Van Etten, 2000; Dorey et al., 2001) might reduce the sensitivity of wild-type abl to low-dose STI571. To test this, we introduced Y412F mutation in wild-type abl-EGFP. Abl-Y412F showed better response to low-dose STI571 than wild-type abl (Fig. 2C). $EC_{50}$ of STI571-induced cell edge translocation of abl-Y412F measured as in Fig. 2B was 1.1 μM. These data are in agreement with our interpretation that phosphorylation at Y412 could reduce the sensitivity of abl-EGFP to low-dose STI571.

**Binding of STI571 probes triggers cell edge translocation of abl.**

The good correspondence between $EC_{50}$ of STI571-induced abl translocation and the known $IC_{50}$ of inhibition of abl by STI571 in cell based assays supports our interpretation that drug-binding drives the translocation of abl probes. To further test whether drug-binding to abl probes is the key to STI571-induced cell edge translocation, we observed the response of the STI571-resistant mutant, abl-T334I, to STI571. T334I mutation, T315I in the abl Ia variant, has frequently been detected among CML patients who developed drug resistant disease. T334 directly interacts with STI571 in the drug binding pocket of abl (Schindler et al., 2000), and is called the gate keeper as T334I shows resistance to most of kinase inhibitors including STI571 (Quintas-Cardama et al., 2007). We found that abl-T334I did not translocate to the leading edge in response to STI571 treatment. Moreover, abl-KD-T334I-EGFP associated with the lamellipodium tip appeared to be displaced by coexpressed abl-KD-mRFP1 upon STI571 treatment

(Fig. 3, supplemental Movie 6). We observed similar adverse effects of STI571 on the cell edge localization between wild-type kinase variants, abl-T334I and abl (data not shown). *In vitro*, T334I shows no significant inhibition at STI571 concentrations 200-fold higher than $IC_{50}$ of wild-type abl (Corbin et al., 2002). In the following comparison on the translocation efficiency between various abl mutants, we used a high concentration of STI571, ~50 μM, to ensure drug binding to abl mutants, some of which are less sensitive to STI571 than wild-type abl. Among those tested, T334I is the only mutant to be resistant to STI571 at 50 μM. In cells coexpressing constructs with and without the T334I mutation, only the wild-type variant presumably binds STI571 and increases its affinity to the partner(s) at the leading edge. This could account for the displacement of T334I from the cell edge upon STI571 treatment. We conclude that drug binding to abl triggers its cell edge translocation.

**Release of N-myristoyl group and the SH3 domain from autoinhibition promote cell edge translocation of abl.**

Given the STI571 binding-induced translocation of abl probes, we were motivated to determine which structures in abl are required for translocation. The effects of various deletions and mutations were validated by direct comparison against coexpressed full-length abl because the degree of STI571-induced translocation varied between cells. We tested deletions and mutations introduced into both wild-type abl and abl-KD, which gave identical results (See below). We used a saturating concentration of STI571, 10-50 μM, to ensure drug binding to abl mutants, some of which are less sensitive to STI571 than wild-type. First, we coexpressed abl-KD-mRFP1 with abl-KD-EGFP, and confirmed identical behaviour and response to STI571 between two constructs (Fig. 4A).

The deletion of the N-terminal CAP (NCAP) domain severely impaired STI571-induced cell edge translocation of abl-KD (Fig. 4B). In abl Ib, a major splice variant of c-abl in human (type IV in mouse), the NCAP region is myristoylated. The myristoylated N-terminal peptide binds the kinase C-lobe (Hantschel et al., 2003; Nagar et al., 2003). We therefore tested the G2A mutant in which glycine at position 2, the target residue for N-myristoylation, had been mutated to alanine. G2A was defective in STI571-induced cell edge translocation (Fig. 4C, supplemental Movie 7). It is of note that both ΔNCAP and G2A were still able to associate with F-actin structures in lamellipodia.

We next tested the A356N mutation in the binding pocket for the myristoyl group. A356N exhibits high kinase activity due to defective autoinhibition (Hantschel et al., 2003). We found that A356N is constitutively associated to the cell edge even prior to STI571 treatment whereas abl-mRFP1 localized to the cell edge only after STI571 perfusion (Fig. 4D, supplemental Movie 8). These data raise a possibility that the myristoyl group released from the kinase domain contributes to the association of abl to the leading edge.

The deletion and point mutations in the SH3 domain have the most extensively been studied as activating mutations (Barila and Superti-Furga, 1998; Jackson and Baltimore, 1989; Van Etten et al., 1995). We tested two point mutations, P131L and P242E/P249E within the SH3 domain and the SH2-kinase linker region, respectively. Both mutant kinases are highly active as a result of impaired autoinhibitory interactions between the two regions. Abl-KD-P131L translocated to the cell edge less efficiently upon STI571 treatment than abl-KD (Fig. 4E). In marked contrast, the P242E/P249E mutant (abl-PP) was constitutively associated to the cell edge before and after STI571 treatment (Fig. 4F, supplemental Movie 9). The P131L mutation may disrupt the association to the SH3

14

domain ligands such as Abi-2, 3BP-1 and Pag/MSP23 (Cicchetti et al., 1995; Dai and Pendergast, 1995; Wen and Van Etten, 1997). These results indicate that release from the intramolecular interaction and subsequent ligand binding of the SH3 domain promote the cell edge translocation of abl.

**An intact last exon region but not its F-actin binding is required for translocation.**

We next tested the motifs downstream of the kinase domain in abl. We observed the behaviour of abl-ΔFB-KD in which C-terminal 32 amino acids are deleted. Deletion of this portion eliminates F-actin binding (Hantschel et al., 2005). Consistently, abl-ΔFB showed diffuse cytoplasmic localization. Upon perfusion of STI571, abl-ΔFB-KD translocated to the cell edge to the same extent as full-length abl-KD (Fig. 4G, supplemental Fig. 2, Movie 10). Thus the cell edge translocation of abl does not require its ability to bind F-actin. This finding is consistent with the decrease in abl or abl-KD signals associated with the actin network upon STI571 treatment (Fig. 1A, D). Further shortening of the C-terminus, which eliminated the entire C-terminal last exon region, did not abolish but substantially reduced STI571-induced translocation (Fig. 4H, supplemental Movie 11). The deleted region includes multiple proline-rich motifs that bind abl ligands such as Crk, Nck and abi-1 (Woodring et al., 2003). Taken together, our data (Fig. 4I) indicate that binding of STI571 to abl induces its cell edge translocation by promoting the complex formation with putative partner(s) through the myristoyl group, the SH3 domain and the last exon region.

**A rapid induction of slow diffusive abl by STI571 revealed by single-molecule observation.**

15

Single-molecule fluorescence microscopy was also useful and elucidated another aspect of STI571-modulated molecular behaviour of abl. In lamellipodia, abl-KD-EGFP visualized as single-molecules at 20 frames/s exhibited two distinct kinetics of dissociation from cellular structures (Fig. 5A). Both species did not show any directional movement. Since our microscopy would detect directional movement of molecules (Higashida et al., 2004) at up to ~10 μm/s under the setting, active transport of abl is unlikely. The slow diffusive species were more predominant at the lamellipodium tip than in the rest of lamellipodia. Our previous studies (Miyoshi et al., 2006; Watanabe and Mitchison, 2002) have used single-molecule 'speckle' microscopy to monitor cytoskeletal association of molecules because immobilization of probes is the key for the formation of discrete speckle signals. We applied the same strategy to distinguish two species. When acquired using the slower exposure time, only a fraction of abl, which mainly consisted of slow diffusive species, were visualized (Fig. 5B, supplemental Movie 12). Images acquired with the 1500 ms exposure revealed that STI571 rapidly increased the slow diffusive abl-KD not only at the tip but also in the body of lamellipodia (Fig. 5C). The number of single-molecule abl-KD-EGFP (Fig. 5C') and abl-EGFP (Fig. 5D) visualized with the slower exposure times (800-1500 ms) increased significantly after perfusion of STI571. Moreover, single-molecule observation revealed the motion of slow diffusive abl near the cell periphery which appears to largely represent random diffusive processes (Fig. 5E, supplemental Movie 13). Together with the critical role of N-myristoylation (Fig. 4C, D), STI571-bound abl most likely accumulates to the lamellipodium tip by co-diffusing with putative partners through multiple interactions including the myristoyl group-membrane interaction, but not by simply being targeted to the preexisting partners at the lamellipodium tip such as

16

abi-1. Extensive biochemical and optical analysis on such diffusive motions of abl is

required to elucidate the underlying mechanisms.

**Discussion**

Using high resolution live-cell imaging approaches, our present study revealed rapid cell edge translocation of abl kinase induced by its inhibitor, STI571 in lamellipodia of XTC fibroblasts. Several lines of evidence indicate that binding of STI571, but not other indirect mechanisms such as dephosphorylation of abl substrates, induces translocation of abl probes. First, the kinase dead mutant of abl (K290M) showed similar translocation in response to STI571. Second, $EC_{50}$ of STI571-induced cell edge translocation of abl is comparable to the known $IC_{50}$ of this drug in other abl-dependent cellular processes. Third, cell edge association of the drug resistant abl-T334I mutant was diminished upon STI571 treatment, presumably displaced by STI571-bound wild-type variants. For efficient translocation, multiple abl structures such as N-myristoylation, the SH3 domain and the last exon region are required. Contrary to the currently prevailing view that STI571 stabilizes the autoinhibited conformation of abl (Nagar et al., 2003; Wang, 2004), our domain analysis (Fig. 4) suggests that STI571 may promote complex formation with putative partner(s) of abl.

The presence of two populations of abl with distinct diffusive behaviours prior to STI571 treatment (Fig. 5A, B) suggests that the conformation of abl in cells is at dynamic equilibrium (Fig. 6). We designate the open, partner-associated state of abl as the 'co-assembled' state. Based on our domain analysis, we postulate that upon binding to STI571, this equilibrium shifts to the co-assembled state in which the myristoyl group and the SH3 domain are disassembled from autoinhibitory interactions. Released myristoyl group and the SH3 domain together with the last exon region may bridge the interactions with putative cellular partner(s) of abl. Such complex presumably interacts with the plasma membrane through the N-myristate attached to abl. STI571-bound abl

18

may then accumulate to the cell periphery by slow diffusive motion. In PKA, binding of the regulatory RII subunit switches the catalytic subunit to expose the N-myristate attached to the catalytic subunit (Gangal et al., 1999). To our knowledge, our finding is the first example of inhibitor-induced conformational regulation of kinases. This STI571-induced inside-out conformation regulation presumably requires abl-interacting molecule(s).

In crystals of STI571-bound abl, the activation loop is stabilized in an inactive conformation (Schindler et al., 2000). This unique conformation is believed to explain specificity of STI571. A recent report, however, has shown that the kinase domain of abl in complex with an ATP-peptide conjugate adopts a different inactive conformation which closely resembles that of src kinases (Levinson et al., 2006). These observations infer flexible nature of the catalytic core of the kinase and its modulation by interacting molecules. The binding of the myristoyl group also induces a conformation change in the kinase C-lobe, causing the C-terminal helix αI to undergo a ~90 degree bend (Nagar et al., 2003). Currently, it is unknown whether STI571 affects the interaction between the kinase and regulatory domains (Nagar et al., 2003). In this regard, it is interesting to note that Nagar et al. (Nagar et al., 2006; Nagar et al., 2003) described crystals of myristoylated abl[1-531] in complex with another inhibitor PD166326 which consisted of two crystallographically independent molecules. One was in the inactive state with the SH3-SH2 unit docked to the kinase domain, and the other was in an elongated conformation with the myristoyl group no longer associating to the kinase domain. This example shows possible conformation fluctuation of inhibitor-bound abl between closed and co-assembled states. The X-ray scattering analysis (Nagar et al., 2006) has indicated that the majority of inhibitor-bound abl is in the closed state. Our findings suggest that

in the presence of cellular factors, STI571 promotes the formation of a complex between abl and partner(s).

Our data show translocation of STI571-bound abl to the lamellipodium tip and the pivotal role of the SH3 domain and the last exon region in this translocation. Abi-1 and abi-2 may be a good candidate for the partner of STI571-bound abl. Abi-1/2 interacts with the SH3 domain and the last exon region of abl. Abi-1 is localized at the lamellipodium tip (Nakagawa et al., 2001) as a component of a protein complex consisting of WAVE/Scar1/2/3, Sra1/PIR121, Nap1 and Hspc300 (Eden et al., 2002). This complex mediates signals from GTP-bound Rac1 and induces nucleation of the dendritic F-actin network in the lamellipodium tip. Abi-1/2 also plays an important role in mediating signaling downstream of abl. Abi-1 promotes tyrosine phosphorylation of WAVE2 (Leng et al., 2005) and Mena (Tani et al., 2003) by bridging the interaction with abl. In hematopoietic cell lines, Bcr-abl induces clustering of an actin-rich structure containing abi-1, WAVE2 and $\beta$1-integrin whereas mutations in Bcr-abl that impairs interaction with abi-1/2 abrogate this cluster formation (Li et al., 2007). The ability for this integrin clustering is correlated with the accumulation of Bcr-abl-transformed myeloid cells in the spleen (Dai et al., 2001). From these properties, abi-1/2 may be referred to as a co-activator of abl kinase (Suzuki and Shishido, 2007). Since STI571 abolishes such adhesion clusters (Li et al., 2007), Bcr-abl-induced adhesion clusters in hematopoietic cells appear to differ from the putative protein complex of STI571-bound abl in XTC cells. On the other hand, abl-interactors such as Pag (Wen and Van Etten, 1997), Rb (Welch and Wang, 1993) and F-actin (Woodring et al., 2001) inhibit the kinase activity of abl. Based on these findings, a co-inhibition mechanism has been proposed for cell factor regulation of abl kinase activity (Wang, 2004). Our current

findings have now opened up another possibility of a two components inhibition mechanism by which cellular cofactor(s) may play a role in the kinase inhibitor modulation of abl functions. To fully understand this mode of cofactor modulation of kinase inhibition, identification of partner(s) for STI571-bound abl and biochemical reconstitution combining abl, kinase inhibitors and such putative partner(s) both in cells and *in vitro* are required.

**Prospects and implications**

The regulation of abl has extensively been studied both biochemically and structurally. Although such analyses have provided a tremendous amount of insights, they were unable to detect our current findings as it will require reconstitution using full-length abl proteins together with putative cellular partner(s). Our current findings imply a possible involvement of such cellular components in the kinase inhibition of abl. All the quantification methods, edge/body fluorescence ratio measurement (Fig. 2), comparison against RFP-tagged full-length variants (Fig. 4) and single-molecule counting (Fig. 5B-D) can be developed into automatic analysis suited to high-content drug screening and target evaluation. Our study highlights that direct observation of molecular behaviour of abl itself and its variants could elucidate the mechanism of action of inhibitors and the influence of mutations readily under live-cell environment.

**Acknowledgment**

We thank Roger Y. Tsien for mRFP1 and mCherry cDNAs; David Baltimore for cDNA
of mouse type IV c-abl and its kinase defective K290M mutant; Novartis Pharma for
supply of STI571; Jun Suzuki for valuable comments and suggestions.

**References**

Azam M, Latek RR and Daley GQ (2003) Mechanisms of autoinhibition and STI-571/imatinib resistance revealed by mutagenesis of BCR-ABL. *Cell* **112**:831-843.

Barila D and Superti-Furga G (1998) An intramolecular SH3-domain interaction regulates c-Abl activity. *Nat Genet* **18**:280-282.

Brasher BB and Van Etten RA (2000) c-Abl has high intrinsic tyrosine kinase activity that is stimulated by mutation of the Src homology 3 domain and by autophosphorylation at two distinct regulatory tyrosines. *J Biol Chem* **275**:35631-35637.

Burton EA, Oliver TN and Pendergast AM (2005) Abl kinases regulate actin comet tail elongation via an N-WASP-dependent pathway. *Mol Cell Biol* **25**:8834-8843.

Campbell RE, Tour O, Palmer AE, Steinbach PA, Baird GS, Zacharias DA and Tsien RY (2002) A monomeric red fluorescent protein. *Proc Natl Acad Sci USA* **99**:7877-7882.

Cicchetti P, Ridley AJ, Zheng Y, Cerione RA and Baltimore D (1995) 3BP-1, an SH3 domain binding protein, has GAP activity for Rac and inhibits growth factor-induced membrane ruffling in fibroblasts. *EMBO J* **14**:3127-3135.

Corbin AS, Buchdunger E, Pascal F and Druker BJ (2002) Analysis of the structural basis of specificity of inhibition of the Abl kinase by STI571. *J Biol Chem* **277**:32214-32219.

23

Dai Z, Kerzic P, Schroeder WG and McNiece IK (2001) Deletion of the Src homology 3 domain and C-terminal proline-rich sequences in Bcr-Abl prevents Abl interactor 2 degradation and spontaneous cell migration and impairs leukemogenesis. *J Biol Chem* **276**:28954-28960.

Dai Z and Pendergast AM (1995) Abi-2, a novel SH3-containing protein interacts with the c-Abl tyrosine kinase and modulates c-Abl transforming activity. *Genes Dev* **9**:2569-2582.

de Klein A, van Kessel AG, Grosveld G, Bartram CR, Hagemeijer A, Bootsma D, Spurr NK, Heisterkamp N, Groffen J and Stephenson JR (1982) A cellular oncogene is translocated to the Philadelphia chromosome in chronic myelocytic leukaemia. *Nature* **300**:765-767.

Dorey K, Engen JR, Kretzschmar J, Wilm M, Neubauer G, Schindler T and Superti-Furga G (2001) Phosphorylation and structure-based functional studies reveal a positive and a negative role for the activation loop of the c-Abl tyrosine kinase. *Oncogene* **20**:8075-8084.

Druker BJ, Tamura S, Buchdunger E, Ohno S, Segal GM, Fanning S, Zimmermann J and Lydon NB (1996) Effects of a selective inhibitor of the Abl tyrosine kinase on the growth of Bcr-Abl positive cells. *Nat Med* **2**:561-566.

Eden S, Rohatgi R, Podtelejnikov AV, Mann M and Kirschner MW (2002) Mechanism of regulation of WAVE1-induced actin nucleation by Rac1 and Nck. *Nature* **418**:790-793.

Gangal M, Clifford T, Deich J, Cheng X, Taylor SS and Johnson DA (1999) Mobilization of the A-kinase N-myristate through an isoform-specific intermolecular switch. *Proc Natl Acad Sci USA* **96**:12394-12399.

Hantschel O, Nagar B, Guettler S, Kretzschmar J, Dorey K, Kuriyan J and Superti-Furga G (2003) A myristoyl/phosphotyrosine switch regulates c-Abl. *Cell* **112**:845-857.

Hantschel O, Wiesner S, Guttler T, Mackereth CD, Rix LL, Mikes Z, Dehne J, Gorlich D, Sattler M and Superti-Furga G (2005) Structural basis for the cytoskeletal association of Bcr-Abl/c-Abl. *Mol Cell* **19**:461-473.

Higashida C, Miyoshi T, Fujita A, Oceguera-Yanez F, Monypenny J, Andou Y, Narumiya S and Watanabe N (2004) Actin polymerization-driven molecular movement of mDia1 in living cells. *Science* **303**:2007-2010.

Jackson P and Baltimore D (1989) N-terminal mutations activate the leukemogenic potential of the myristoylated form of c-abl. *EMBO J* **8**:449-456.

Jin H and Wang JY (2007) Abl tyrosine kinase promotes dorsal ruffles but restrains

lamellipodia extension during cell spreading on fibronectin. *Mol Biol Cell* **18**:4143-4154.

Kantarjian H, Sawyers C, Hochhaus A, Guilhot F, Schiffer C, Gambacorti-Passerini C, Niederwieser D, Resta D, Capdeville R, Zoellner U, Talpaz M, Druker B, Goldman J, O'Brien SG, Russell N, Fischer T, Ottmann O, Cony-Makhoul P, Facon T, Stone R, Miller C, Tallman M, Brown R, Schuster M, Loughran T, Gratwohl A, Mandelli F, Saglio G, Lazzarino M, Russo D, Baccarani M and Morra E (2002) Hematologic and cytogenetic responses to imatinib mesylate in chronic myelogenous leukemia. *N Engl J Med* **346**:645-652.

Kurokawa K, Mochizuki N, Ohba Y, Mizuno H, Miyawaki A and Matsuda M (2001) A pair of fluorescent resonance energy transfer-based probes for tyrosine phosphorylation of the CrkII adaptor protein in vivo. *J Biol Chem* **276**:31305-31310.

Leng Y, Zhang J, Badour K, Arpaia E, Freeman S, Cheung P, Siu M and Siminovitch K (2005) Abelson-interactor-1 promotes WAVE2 membrane translocation and Abelson-mediated tyrosine phosphorylation required for WAVE2 activation. *Proc Natl Acad Sci U S A* **102**:1098-1103.

Levinson NM, Kuchment O, Shen K, Young MA, Koldobskiy M, Karplus M, Cole PA and Kuriyan J (2006) A Src-like inactive conformation in the abl tyrosine kinase domain. *PLoS Biol* **4**:e144.

Li Y, Clough N, Sun X, Yu W, Abbott BL, Hogan CJ and Dai Z (2007) Bcr-Abl induces abnormal cytoskeleton remodeling, beta1 integrin clustering and increased cell adhesion to fibronectin through the Abl interactor 1 pathway. *J Cell Sci* **120**:1436-1446.

Miyoshi T, Tsuji T, Higashida C, Hertzog M, Fujita A, Narumiya S, Scita G and Watanabe N (2006) Actin turnover-dependent fast dissociation of capping protein in the dendritic nucleation actin network: evidence of frequent filament severing. *J Cell Biol* **175**:947-955.

Nagar B, Hantschel O, Seeliger M, Davies JM, Weis WI, Superti-Furga G and Kuriyan J (2006) Organization of the SH3-SH2 unit in active and inactive forms of the c-Abl tyrosine kinase. *Mol Cell* **21**:787-798.

Nagar B, Hantschel O, Young MA, Scheffzek K, Veach D, Bornmann W, Clarkson B, Superti-Furga G and Kuriyan J (2003) Structural basis for the autoinhibition of c-Abl tyrosine kinase. *Cell* **112**:859-871.

Nakagawa H, Miki H, Ito M, Ohashi K, Takenawa T and Miyamoto S (2001) N-WASP, WAVE and Mena play different roles in the organization of actin cytoskeleton in lamellipodia. *J Cell Sci* **114**:1555-1565.

Pendergast AM (2002) The Abl family kinases: mechanisms of regulation and signaling. *Adv Cancer Res* **85**:51-100.

Quintas-Cardama A, Kantarjian H and Cortes J (2007) Flying under the radar: the new wave of BCR-ABL inhibitors. *Nat Rev Drug Discov* **6**:834-848.

Roumiantsev S, Shah NP, Gorre ME, Nicoll J, Brasher BB, Sawyers CL and Van Etten RA (2002) Clinical resistance to the kinase inhibitor STI-571 in chronic myeloid leukemia by mutation of Tyr-253 in the Abl kinase domain P-loop. *Proc Natl Acad Sci USA* **99**:10700-10705.

Schindler T, Bornmann W, Pellicena P, Miller WT, Clarkson B and Kuriyan J (2000) Structural mechanism for STI-571 inhibition of abelson tyrosine kinase. *Science* **289**:1938-1942.

Shaner NC, Campbell RE, Steinbach PA, Giepmans BN, Palmer AE and Tsien RY (2004) Improved monomeric red, orange and yellow fluorescent proteins derived from Discosoma sp. red fluorescent protein. *Nat Biotechnol* **22**:1567-1572.

Shi Y, Alin K and Goff SP (1995) Abl-interactor-1, a novel SH3 protein binding to the carboxy-terminal portion of the Abl protein, suppresses v-abl transforming activity. *Genes Dev* **9**:2583-2597.

Suzuki J and Shishido T (2007) Regulation of cellular transformation by oncogenic and normal Abl kinases. *J Biochem* **141**:453-458.

Tani K, Sato S, Sukezane T, Kojima H, Hirose H, Hanafusa H and Shishido T (2003)

Abl interactor 1 promotes tyrosine 296 phosphorylation of mammalian enabled (Mena) by c-Abl kinase. *J Biol Chem* **278**:21685-21692.

Ting AY, Kain KH, Klemke RL and Tsien RY (2001) Genetically encoded fluorescent reporters of protein tyrosine kinase activities in living cells. *Proc Natl Acad Sci USA* **98**:15003-15008.

Van Etten RA, Debnath J, Zhou H and Casasnovas JM (1995) Introduction of a loss-of-function point mutation from the SH3 region of the Caenorhabditis elegans sem-5 gene activates the transforming ability of c-abl in vivo and abolishes binding of proline-rich ligands in vitro. *Oncogene* **10**:1977-1988.

Wang JY (2004) Controlling Abl: auto-inhibition and co-inhibition? *Nat Cell Biol* **6**:3-7.
Watanabe N and Mitchison TJ (2002) Single-molecule speckle analysis of actin filament turnover in lamellipodia. *Science* **295**:1083-1086.

Welch PJ and Wang JY (1993) A C-terminal protein-binding domain in the retinoblastoma protein regulates nuclear c-Abl tyrosine kinase in the cell cycle. *Cell* **75**:779-790.

Wen ST and Van Etten RA (1997) The PAG gene product, a stress-induced protein with antioxidant properties, is an Abl SH3-binding protein and a physiological inhibitor of c-Abl tyrosine kinase activity. *Genes Dev* **11**:2456-2467.

Woodring PJ, Hunter T and Wang JY (2001) Inhibition of c-Abl tyrosine kinase activity by filamentous actin. *J Biol Chem* **276**:27104-27110.

Woodring PJ, Hunter T and Wang JY (2003) Regulation of F-actin-dependent processes by the Abl family of tyrosine kinases. *J Cell Sci* **116**:2613-2626.

Woodring PJ, Litwack ED, O'Leary DD, Lucero GR, Wang JY and Hunter T (2002) Modulation of the F-actin cytoskeleton by c-Abl tyrosine kinase in cell spreading and neurite extension. *J Cell Biol* **156**:879-892.

**FOOTNOTES**

MOL #51706

**Figure legends**

**Fig. 1.**

STI571-induced cell edge translocation of abl kinase. (A) Abl-EGFP shows association

with F-actin structures in lamellipodia of XTC fibroblasts. Note the enhanced signals at

the tip of lamellipodia. (B) Rapid increases in abl-EGFP signals at the lamellipodium tip

(arrows) as well as at the punctate actin rich foci induced by STI571 treatment. Images

of abl-EGFP in two XTC cells treated with increasing concentrations of STI571 are

paneled. In addition, cells overexpressing abl-EGFP (lower panels) showed impaired

cell spreading onto poly-lysine-coated glass coverslips, which was relieved by STI571

treatment. (C) Untagged full-length abl also translocated to the lamellipodium tip upon

in XTC cells treated with 1 μM STI571 for 5 min (right panels). F-actin visualized by

fluorescent phalloidin is also shown. Arrows indicate the cells transfected with

pcDNA3-abl. (D) Translocation of the kinase dead K290M mutant (abl-KD) induced by

STI571. Images of abl-EGFP (upper) and abl-KD-mRFP1 (lower), and their merged

image (EGFP, green; mRFP1, red) (right) are shown. Time is duration of 50 μM STI571

treatment. Note the identical distribution of wild-type abl and abl-KD. (E)

Abl-KD-EGFP and mRFP1-actin in cells treated with 50 μM STI571. The panels show

images before and 120 sec after STI571 perfusion. The graphs show the fluorescence

intensity of abl-KD-EGFP (green) and mRFP1-actin (red) along the dotted line. (F)

Abl-KD-EGFP (right) and mRFP1 (left) in cells treated with 50 μM STI571. The

increase in the abl-KD-EGFP signal at the cell periphery is not due to cell shape change.

Scale bars, 5 μm.

**Fig. 2.**

Dose-response analysis of STI571-induced translocation of abl using a computer-assisted method. (A) Cells expressing abl-KD-EGFP were treated with increasing doses of STI571. Right panels show abl-KD-EGFP (green) and the measured area automatically assigned for the lamellipodium edge region (blue) and the body region (red). The graph shows the ratio of the average fluorescence intensity of abl-KD-EGFP between the edge area and the body area (n = 6 cells). Error bars show s.d. The dose-response curve (inset) yields 0.81 $\mu$M for $EC_{50}$. (B) Dose-response analysis of STI571-induced cell edge translocation of wild-type abl-EGFP measured as in A, except that cells were treated with single-dose STI571 (n = 3~4 cells for each STI571 concentration). Error bars show s.d. The dose-response curve for the fold-increase between before and 5 min in edge/body fluorescence ratio (inset) yields 1.8 $\mu$M for $EC_{50}$. (C) A tyrosine to phenylalanine mutation at Y412 in wild-type abl, the phosphorylation of which impairs STI571 binding (Schindler et al., 2000), increased sensitivity to low-dose STI571 treatment. The graph shows the edge/body fluorescence ratio in a cell treated with 0.5 $\mu$M STI571. Only abl-Y412F shows the gradual increase in the ratio. The $EC_{50}$ of STI571-induced cell edge translocation of abl-Y412F-EGFP measured as in B was 1.1 $\mu$M. Scale bars, 5 $\mu$m.

**Fig. 3.**

Displacement of STI571-resistant T334I mutant from the lamellipodium tip upon STI571 treatment; evidence of STI571 binding triggering translocation of abl. Images of abl-KD-mRFP1 and abl-KD-T334I-EGFP before and 60 sec after 50 $\mu$M STI571 treatment are shown. The graph shows the ratio of fluorescence intensity between the lamellipodium edge and body areas measured as in E. Note the adverse effects of

STI571 on two probes; STI571 treatment increased the edge: body ratio of abl-KD and

decreased that of the T334I mutant. Scale bars, 5 μm.


**Fig. 4.**

Roles of N-myristoylation, the SH3 domain and the last exon region in STI571-induced

translocation of abl. Comparisons against coexpressed full-length abl-mRFP1 are shown.

The graphs show fluorescence intensity along the dotted lines. (A) Comparison between

abl-KD-mRFP1 and abl-KD-EGFP 30 sec after perfusion of 50 μM STI571. The graph

shows identical distribution of EGFP- and mRFP1-tagged full-length probes. (B)

Comparison between abl-KD-mRFP1 and ΔNCAP-abl-KD-EGFP 5 min after perfusion

of 50 μM STI571, showing negligible cell edge translocation of ΔNCAP-abl-KD. (C)

Comparison between abl-mRFP1 and abl-G2A-EGFP before and 60 sec after perfusion

of 30 μM STI571, showing negligible cell edge translocation of G2A. (D) Comparison

between abl-mRFP1 and abl-A356N-EGFP before and 180 sec after perfusion of 50 μM

STI571, showing the constant association of A356N with the lamellipodium tip

regardless of STI571 treatment. (E) Less efficient cell edge translocation of the

abl-KD-P131L than abl-KD in response to 50 μM STI571. (F) Comparison between

abl-mRFP1 and abl-PP-EGFP (P242E/P249E) before and 120 sec after perfusion of 50

μM STI571, showing constant association of abl-PP to the lamellipodium tip regardless

of STI571 treatment. (G) Comparison between abl-KD-mRFP1 and abl-KD-ΔFB-EGFP

before and 60 sec after perfusion of 50 μM STI571. Abl-KD-ΔFB showed diffuse

cytoplasmic localization but translocated to a similar degree as abl-KD in response to

STI571. (H) The panels show abl-KD-mRFP1 and abl-KD-ΔC-EGFP before and 60 sec

after perfusion of 50 μM STI571. Note the less marked cell edge translocation of

abl-KD-ΔC than abl-KD. (I) Summary of the effects of mutations in abl on its STI571-induced cell edge translocation and association with the F-actin network. The upper scheme shows the structure of type IV mouse c-abl. Dashed arrows indicate autoinhibitory interactions between the myristoyl group and the kinase C-lobe (purple) and between the SH3 domain and the SH2-kinase linker (green). 'WT or K290M (grey)' indicates that the mutations in both wild-type kinase and abl-KD gave identical results. The kinase dead form of G2A was not tested. For A356N and PP, '+→+' indicates that the mutants are constitutively associated with the lamellipodium tip before and after STI571 treatment. For T334I, '±→-' indicates its weak association to the cell edge which was diminished after STI571 treatment, presumably displaced by coexpressed wild-type variants. Scale bars, 5 μm.

**Fig. 5.**

Rapid induction of slow diffusive species of abl by STI571 revealed by single-molecule imaging. (A) The graphs show the decay in the number of single-molecule abl-KD-EGFP speckles identified at the 1st frame of timelapse images acquired at 50 ms intervals. Molecules associated to the cell contour (lamellipodium tip; magenta) were analyzed separately. Cells treated with 50 μM STI571 for 5-15 min were analyzed on the right graphs. Coloured lines show the data after normalization for photobleaching. Dashed lines indicate the double exponential fit to the data. The best fit was obtained as follows; before treatment; $T_{1/2}$ = 51 ms (62%) and $T_{1/2}$ = 650 ms (38%) at the lamellipodium tip; $T_{1/2}$ = 58 ms (94%) and $T_{1/2}$ = 1700 ms (5.9%) in the body. After treatment; $T_{1/2}$ = 67 ms (50%) and $T_{1/2}$ = 560 ms (50%) at the lamellipodium tip; $T_{1/2}$ = 64 ms (85%) and $T_{1/2}$ = 660 ms (15%) in the body. N = 5 cells for each condition. (B)

Image of XTC cells expressing a low level of abl-KD-EGFP were acquired by varying exposure times. On the right, illumination was attenuated to ~12.5% of the left. Note that only a fraction of abl-KD speckles were visualized as a discrete spot (marked by magenta circles) with the 1500 ms exposure. (C and C') The number of abl-KD-EGFP speckles visualized with the 1500 ms exposure time (marked by magenta circles) increased rapidly upon 50 μM STI571 perfusion. Each colour in the graph indicates data from the same cell (n = 6 cells). **$p$ = 0.002, two-tailed paired $t$-test. (D) The number of abl-EGFP speckles visualized with the 800 ms exposure time increased 2 min after 5 μM STI571 perfusion. Each colour in the graph indicates data from the same cell (n = 6 cells). **$p$ = 0.0088, two-tailed paired $t$-test. (E) Images of single-molecule abl-KD-EGFP speckles in the presence of 10 μM STI571 were panelled at 100 ms intervals. Note the slow diffusive motion of an abl-KD speckle (arrowheads) traveling in the cell edge region (see also supplemental Movie 13). Scale bars, 5 μm.

**Fig. 6.**

Model for possible allosteric regulation and complex formation of abl with putative partner(s) induced by STI571. The structure of abl is depicted by NCAP, SH3, SH2, kinase and F-actin binding (FB) domains and the amino acids important for autoinhibition. Our data suggest that abl exists at least in two different closed (left) and open (right) states. Since our data imply co-assembly with putative partners (X) on the right, we designate this open state as the 'co-assembled' state. These two species of abl in cells is probably at dynamic equilibrium although there might be more complex regulation between the closed and open states (Hantschel et al., 2003). The left species are fast diffusive and transiently interacting with the F-actin network throughout

lamellipodia. The right co-assembled species are slowly diffusive and concentrated to the cell edge. Upon binding to STI571, this equilibrium shifts to the right in which released myristoyl group and the SH3 domain together with the last exon region of abl may bridge the interactions with putative cellular partner(s), X. The right complex may interact also with the plasma membrane through the N-myristate of abl and accumulates to the cell periphery by a diffusion mechanism.
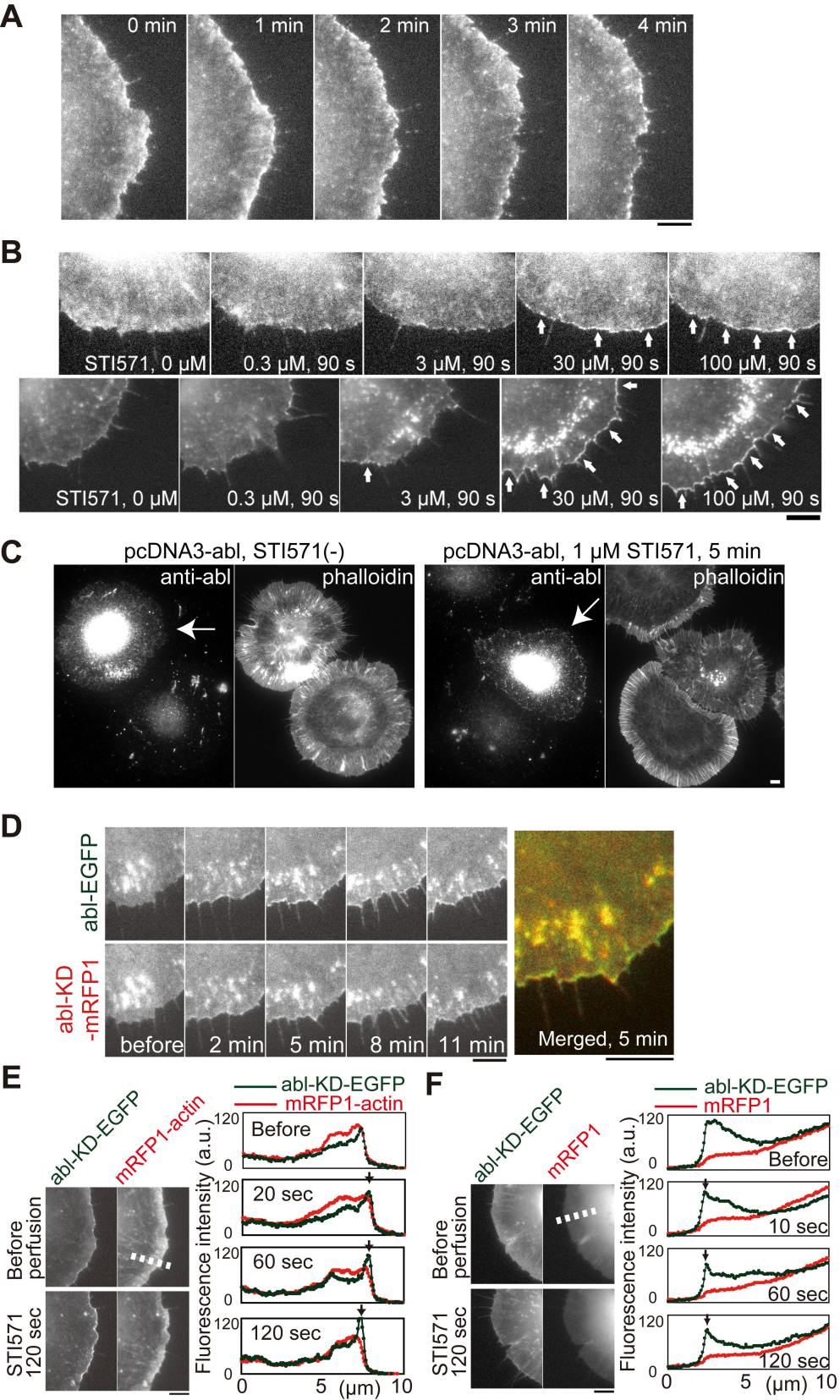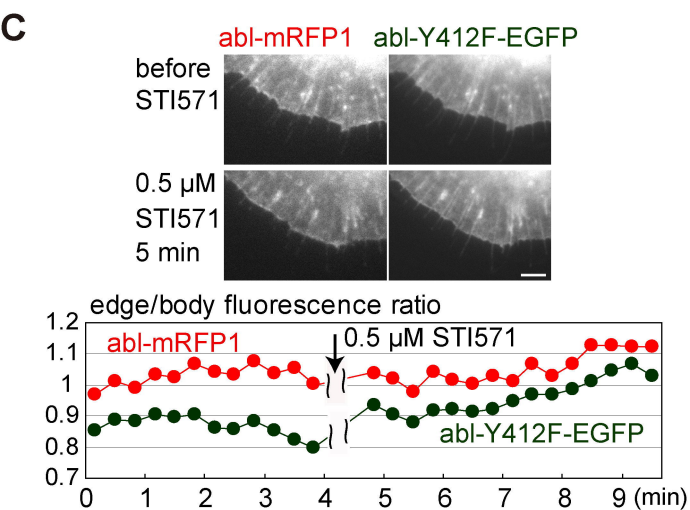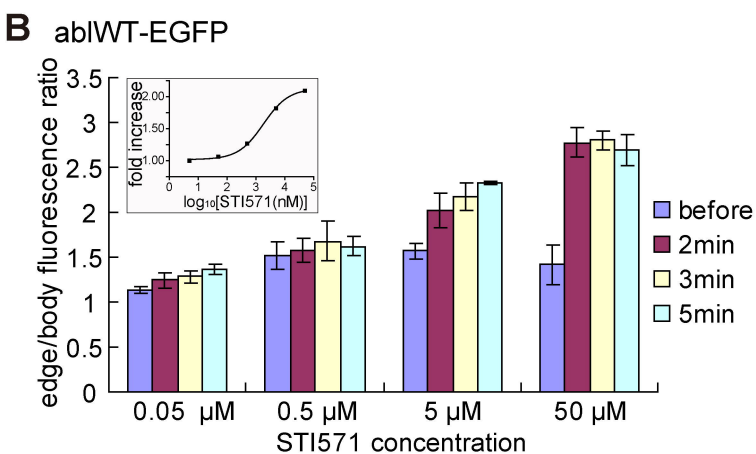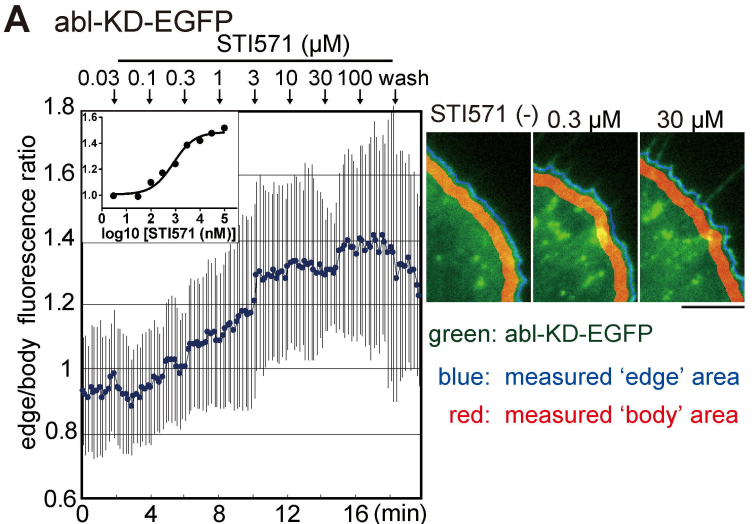
**A** 0 min | 1 min | 2 min | 3 min | 4 min

**B** STI571, 0 μM | 0.3 μM, 90 s | 3 μM, 90 s | 30 μM, 90 s | 100 μM, 90 s

STI571, 0 μM | 0.3 μM, 90 s | 3 μM, 90 s | 30 μM, 90 s | 100 μM, 90 s

**C** pcDNA3-abl, STI571(-) | pcDNA3-abl, 1 μM STI571, 5 min

anti-abl | phalloidin | anti-abl | phalloidin

**D** abl-EGFP

abl-KD-mRFP1

before | 2 min | 5 min | 8 min | 11 min | Merged, 5 min

**E** abl-KD-EGFP | mRFP1-actin

abl-KD-EGFP
mRFP1-actin

Before perfusion

STI571 120 sec

Fluorescence intensity (a.u.)

Before

20 sec

60 sec

120 sec

0 | 5 | 10 (μm)

**F** abl-KD-EGFP | mRFP1

abl-KD-EGFP
mRFP1

Before perfusion

STI571 120 sec

Fluorescence intensity (a.u.)

Before

10 sec

60 sec

120 sec

0 | 5 | 10 (μm)

*Figure 1*

**A** abl-KD-EGFP

STI571 (μM)

0.03 0.1 0.3 1 3 10 30 100 wash

green: abl-KD-EGFP
blue: measured 'edge' area
red: measured 'body' area

**B** ablWT-EGFP

- before
- 2min
- 3min
- 5min

STI571 concentration

**C** abl-mRFP1    abl-Y412F-EGFP

before
STI571

0.5 μM
STI571
5 min
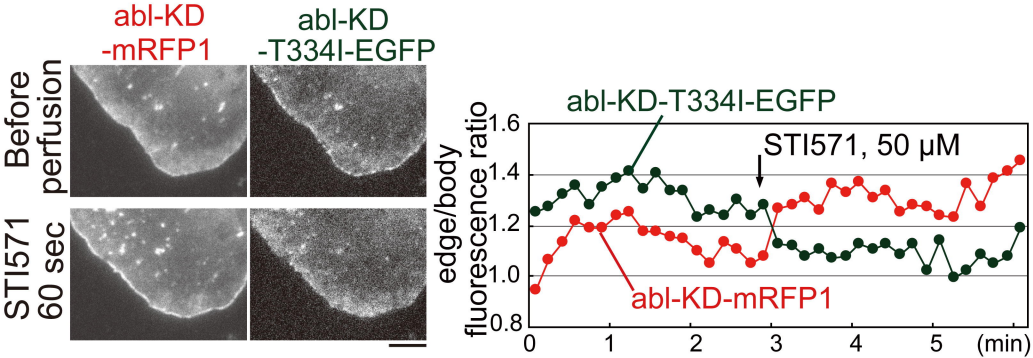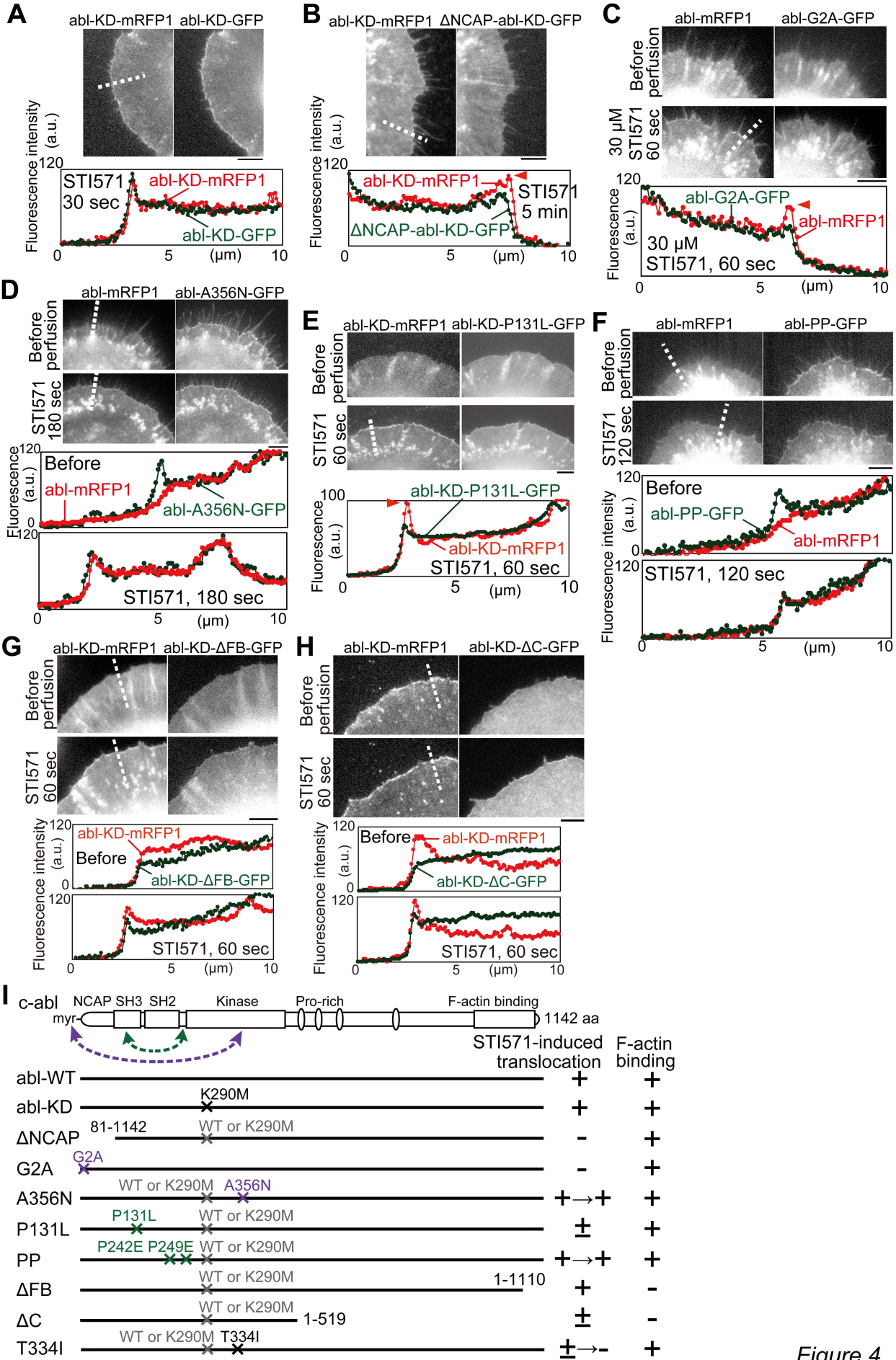
edge/body fluorescence ratio

abl-mRFP1    0.5 μM STI571

abl-Y412F-EGFP

*Figure 2*

*Figure 3*

Figure 4

*Figure 5*

*Figure 6*